Metal-oxide interactions for infiltrated Ni nanoparticles on A-site deficient $La_xSr_{1-3x/2}TiO_3$

Jianing Hui, Dragos Neagu, David Miller, Xiangling Yue, Chengsheng Ni, John T.S. Irvine*
School of Chemistry, University of St Andrews, North Haugh, St Andrews, Fife KY16 9ST, UK

Abstract:
Enhancing the stability of introduced metal catalysts on oxide surfaces is a major issue for infiltrated anodes in Solid Oxide Cells (SOC) and other related catalysis field. Stoichiometric $SrTiO_3$ (STO) and A-site cation deficient $La_xSr_{1-3x/2}TiO_3$ (LST) were compared to investigate the influence of stoichiometry upon the contact between metal and oxide, in order to improve the bonding of catalyst and substrate. Optimization of oxidizing and reducing temperatures for Ni infiltration processes was performed to get good nanoparticles distribution on the perovskite surface. Thermogravimetry (TG) and X-ray diffraction (XRD) analysis showed the formation of NiO, Ni after oxidation and reduction, respectively. Energy Dispersive Spectroscopy (EDS) on a Transmission Electron Microscopy (TEM) was employed to characterize the nickel nanoparticles on the LST surface. No obvious elemental transfer happened between Ni and LST. The TEM images showed Ni nanoparticles bonded well to the A-site deficient perovskite with large contact area. TG analysis in reducing atmosphere indicates interactions between metal-oxide interactions in deficient samples. This may improve the Ni distribution on perovskite surface and further control the growth of Ni particles when heated at extreme temperature.

1. Introduction:

Infiltration is a widely-used method for electrode fabrication in Solid Oxide Fuel Cell (SOFC) and Solid Oxide Electrolysis Cell (SOEC), which allows high flexibility in the choice of catalysts and great control of the microstructure [1,2]. For the fuel electrode used in Solid Oxide Cells (SOC), sufficient electronic and ionic conductivity are required to ensure reaction happens at triple phase boundary (TPB). Moreover, good electrocatalytic activity is important to reduce overpotential and then enhance performance. An often-used strategy is to fabricate a porous skeleton, which could be an ionic conductor (like YSZ [3]), an electronic conductor (like LSCT [4]) or a mixed ionic electronic conductor (like LSCM [5]), where catalysts are infiltrated on the surface of the skeleton. By controlling the concentration of precursor solution and cycling procedures, homogeneously distributed nano-sized catalysts could be achieved [6]. However, one drawback to this method is the degradation caused by coking and metal agglomeration at ceramics surface due to the poor interface bonding between catalysts and oxide substrates [7, 8].

To prevent Ni sintering at elevated temperature where SOC works, two main strategies were employed. One is to control the distribution of metal catalysts by optimizing Ni contents and cycling procedures, though without significant improvement for long term test [6]. On the other hand, looking for a suitable substrate that can better anchor catalyst particles on its surface seems a more promising way. A-site deficient La doped $SrTiO_3$ has been investigated as a candidate for SOFC and SOEC electrode due to its good conductivity and stability under reducing atmosphere [9, 10]. A recent study by Neagu and Irvine illustrated that nanoparticles exsolved from A-site deficient LST present good coking resistance. The Ni particles formed by cations diffuse from the lattice to the surface remain bonded to the parent perovskite [11, 12]. Based on this, we propose that cation deficiency may enable atomic transfer and then enhance bonding between metal and oxide in the process of Ni immigration.

In this study, the influence of A-site deficiency on metal oxide interaction was investigated on a Ni infiltrated $La_xSr_{1-3x/2}TiO_3$ (x=0, 0.1, 0.2) substrate. We aim to obtain strong metal oxide interface bonding by tuning the cation deficiency in titanate perovskite.

2. Experimental

2.1 Materials synthesis

Samples of $SrTiO_3$ (STO), $La_{0.2}Sr_{0.7}TiO_3$ (LST27), $La_{0.4}Sr_{0.4}TiO_3$ (LST44) were prepared via solid state synthesis. High purity raw materials were dried at different temperatures (La_2O_3 at 850, SrO and TiO_2 at 350) before weighing. A stoichiometric quantity of dry powders was mixed in acetone. To break the agglomerates into fine powders, an ultrasonic probe (Hielscher UP200S) was applied with amplitude at 0.5 and cycle at 0.6. Additionally, a small quantity of dispersant (KD-1, 1 wt%) was added into the mixture to get a better

suspension. After 20 minutes ultrasonic treatment the homogeneous suspension was dried on a hot plate (50 °C) with magnetic stirring. The dried powder was calcined at 1000 °C in air for 12 h before ball milling on a planetary ball mill machine (Fritsch Pulverisette) with 10 mm zirconia balls. Re-dried powder was pressed uniaxially into pellets and sintered at 1450 °C in air for 12 h. Porous pellets were prepared by mixing sintered powder and pore former (flour) homogeneously and then sintered at 1450 °C in air for 5 h.

2.2 Impregnation

Nickel nitrate solution (3 M, in ethanol) was used for impregnation. For porous samples, nitrate solution was dropped onto the sample and dried. But for dense samples, a spin coating method was employed to remove excess solution to avoid agglomeration on the small surface. All the samples after infiltration were calcined in air to decompose nitrate to oxide. After that, it was reduced in 5% H_2 at proper temperature to get Ni particles. The influence of oxidizing and reducing temperature has been studied here.

2.3 Analytical techniques

The crystal structure and phase purity was confirmed by X ray powder diffraction on a PANalytical Empyrean Reflection Diffractometer (Cu Kα1 radiation). The obtained XRD patterns were analysed with HighScore Plus software to check crystal structure. The microstructures of materials were observed with a field emission scanning electron microscope (SEM, JEOL, JSM 6700) and transition electron microscope (TEM, JEOL, JEM 2001). Thermogravimetric analysis was done on a Netzsch Model STA 449C instrument.

3. Results and discussion

3.1 $La_xSr_{1-3x/2}TiO_3$

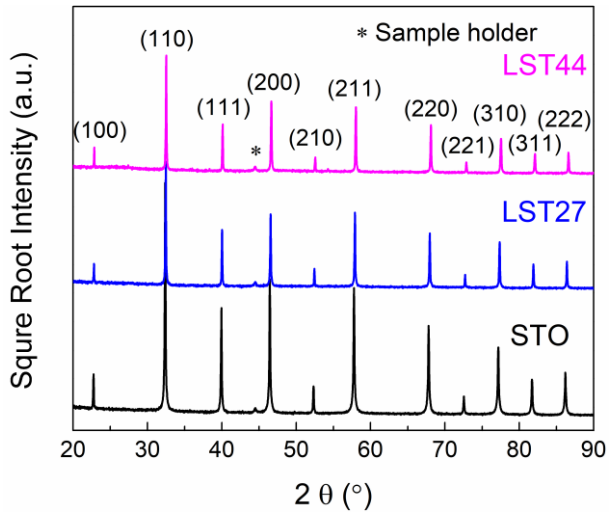

Figure 1. Room temperature powder diffraction patterns collected for $La_xSr_{1-3x/2}TiO_3$ (x=0, 0.1, 0.2).

An un-doped $SrTiO_3$ has cubic structure without any distortion in lattice. After introducing dopants into the lattice, to replace Sr with La on A-site, the crystal structure changes to a lower symmetry phase because of oxygen octahedral tilt. The XRD patterns in Figure 1 show these three perovskites with different A site deficiency are in same structure (looks like cubic) without any secondary phase. However, the intensity of high deficient samples is a bit lower than the stoichiometric one as shown in Figure 2. This indicates slight lattice disorder exists in A-site deficient samples that weakens the X-ray diffraction effect. In high deficient sample LST44, a tiny peak was found at 38.3°, which can be indexed to out of phase tilt of oxygen octahedral upon CJ Howard's work [13] in tetragonal symmetry. This suggests a trend that the cubic perovskite changes to lower symmetry when introducing more A site deficiency by doping La. Besides, more cation vacancies results in reflection peak shifts to small d-spacing area. This could be explained by the loss of cation leading to lattice shrinkage. The volume of pseudo cubic unit cell was expected to decrease as cation deficiency increases.

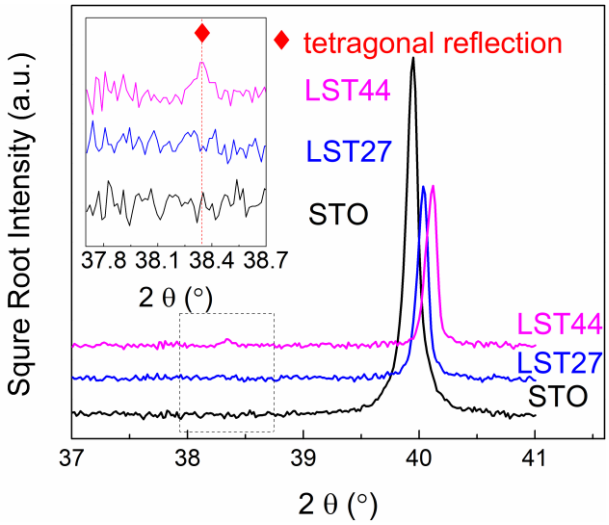

Figure 2. Details of peak (111) in XRD patterns collected from powder.

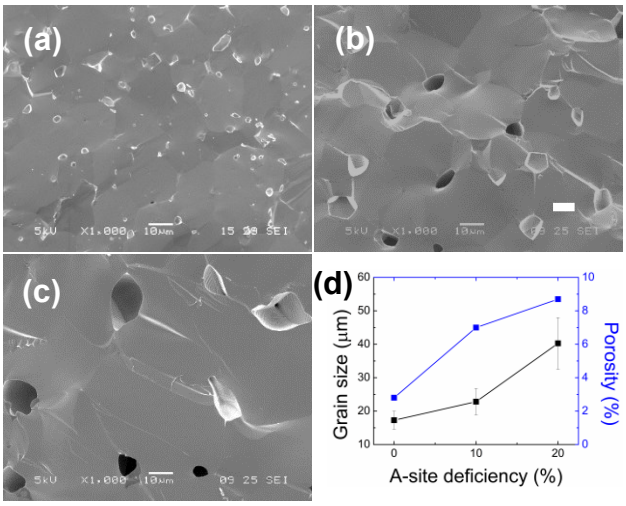

Figure 3. Cross-section morphology of as-prepared pellets $La_xSr_{1-3x/2}TiO_3$, x=0 (a), 0.1 (b), 0.2 (c); (d) the grain size and porosity of pellets as a function of the A-site deficiency. Scale bar is 10 μm.

The morphology of LST cross-section surface has been characterized by FESEM, which are shown in Figure 3. All these samples show a clean surface, without any secondary phase segregation along the grain boundary. Moreover, obvious grain growth was found in high deficiency samples. This gives indications that vacancies on the A site may promote cations diffusion at elevated temperature. This effect may play a role in metal-oxide interaction during infiltration processes.

3.2 Infiltration

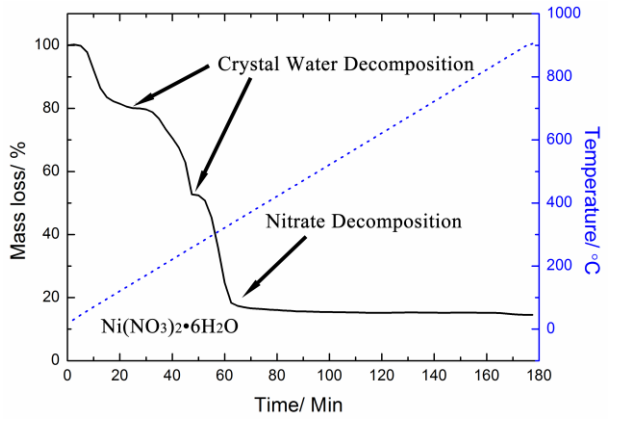

Figure 4. Mass change of $Ni(NO_3)_2{\cdot}6H_2O$ heated from room temperature to 900 °C in air.

Nickel nitrate ($Ni(NO_3)_2{\cdot}6H_2O$), the precursor of infiltration, was calcined in a Thermogravimetry instrument in air to study its decomposition process. The result in Figure 4 shows the nitrate decomposed to be NiO completely at around 400 °C. To get a proper infiltration heating temperature for the LST substrate, optimisation experiments were carried out on dense LST44 pellet.

Firstly, the oxidizing temperature was fixed at 500 °C, and then five samples with NiO were reduced at different temperature from 500 °C to 900 °C. In Figure 5, particles reduced at 500 °C were still in anomalous shape, which means NiO was not reduced totally. From 700 °C, the particles became regular sphere shape indicates pure Ni metal formation. After even higher temperature reduction, the small nanoparticles started to disappear, especially at 900 °C. This may because of Ni sintering at elevated temperature. It seems the temperature zone from 600 °C to 800 °C is suitable for reduction. Finally, 700 °C was used in our study.

Secondary, oxidising temperature was also optimized in the same way. Ni infiltrated LST44 calcined at 500 °C, 700 °C and 900 °C were reduced at 700 °C for 1 hour to compare the particle distribution. When oxidized at 500 °C, the NiO was very porous and in layer structure. Hence, particles agglomerated during Ni formation and results in large particles. On the other hand, high temperature calcination in air can cause NiO sintering and lead to large NiO particle size as well. It was found that 700 °C oxidation in air followed with reduction at same temperature can produce well controlled Ni nanoparticle distribution on LST surface.

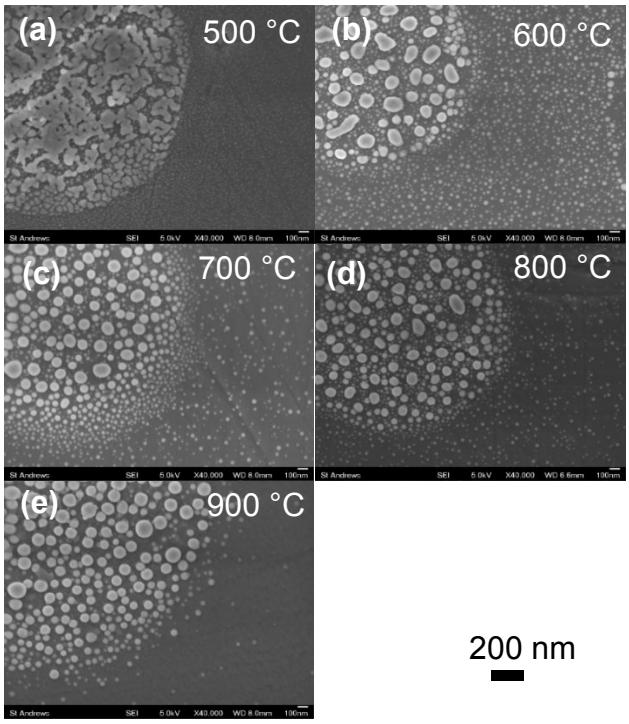

Figure 5. Morphology of Ni infiltrated LST44 when oxidized at 700 °C and then reduced in 5% H_2 at different temperature (From 500 °C to 900 °C).

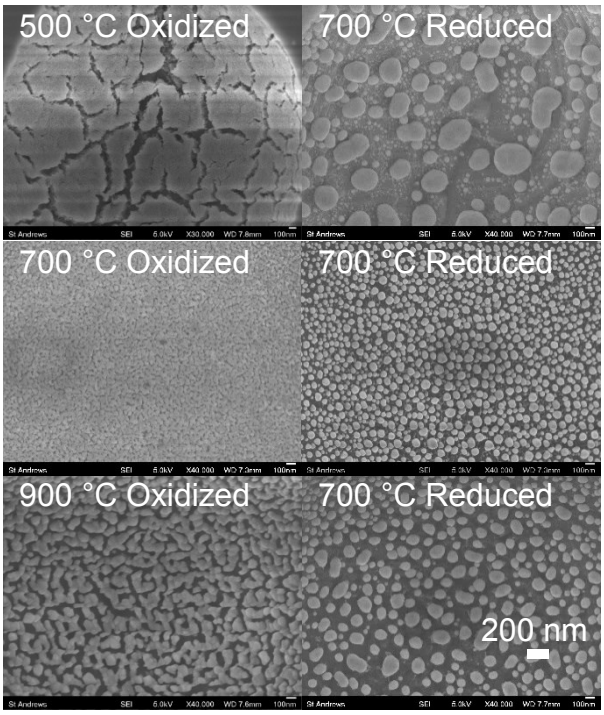

Figure 6. Morphology of Ni infiltrated LST44 when oxidized at different temperature (From 500 °C to 900 °C) and then reduced in 5% H_2 at 700 °C.

X-ray diffraction study on porous STO and LST44 substrate was done to monitor the phase change during infiltration procedures. After oxidation in air at 700 °C, weak NiO peaks appear at 37.3° and 43.3°. These two reflections disappear after reduction in 5% H_2, while the intensity of 44.5° peak increases. It comes from the Ni f.c.c. phase. Unfortunately, it overlaps with Fe f.c.c. reflection peak from the steel sample holder. No other peaks were found during these heating processes, which suggests Ni and LST are not easy to react with each other at temperature lower than 900 °C no matter in air or 5% H_2.

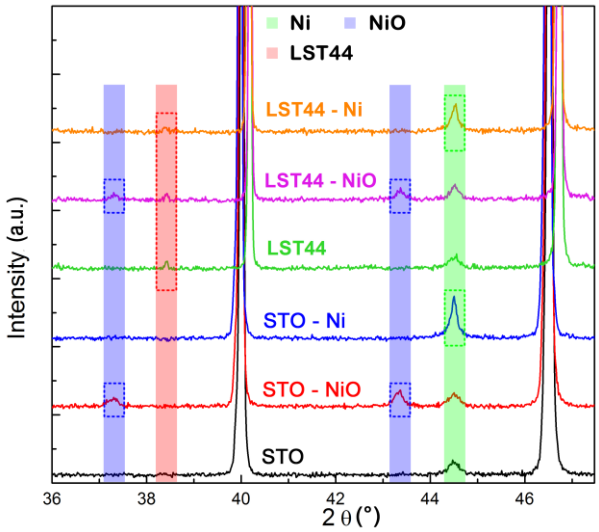

Figure 7. X-ray diffraction patterns of Ni infiltrated porous STO and LST44 after oxidation in air and reduction in 5% H_2 at 700 °C.

3.3 Metal oxide interaction

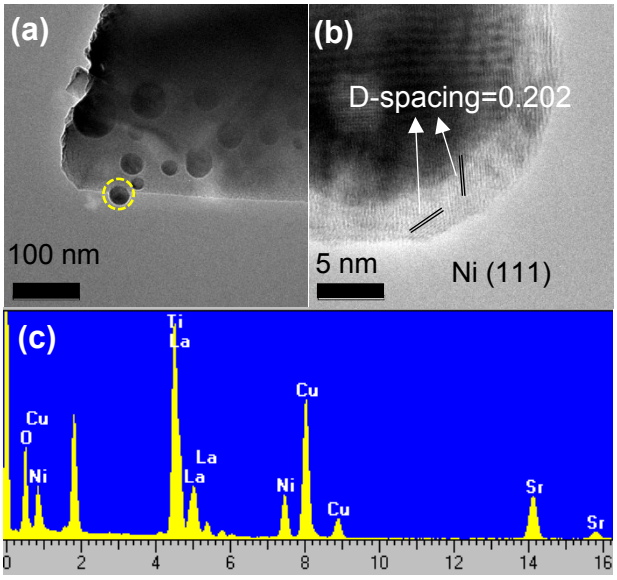

Figure 8. TEM images of Ni infiltrated LST44: (a) overall morphology; (b) high resolution image of Ni particle; (c) EDX spectrum of Ni particle. Infiltrated sample was oxidized at 700 °C for 3 h and then reduced at 700 °C for 3 h.

The TEM image in Figure 8 shows LST44 modified with one small Ni nanoparticle. The interface between metal and oxide is clear, which presents quite good bonding with large contact area. Fourier transform of the high-resolution image indicates a single crystal within this Ni particle. Moreover, d-spacing measured in the image is about 0.2027 Å, which can be identical to (111) plane in f.c.c. Ni phase. This corresponds well to the XRD results in Figure 7. EDS spectrum further confirmed that Ni particle formed on the LST44 surface. Here, the copper signal comes from TEM grid.

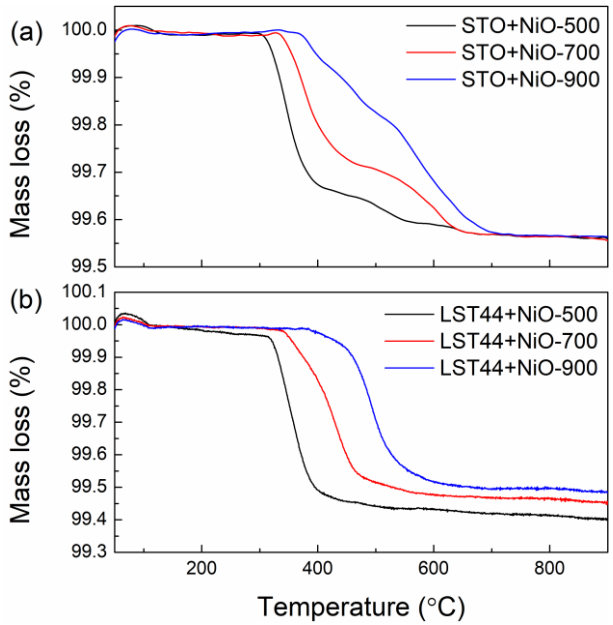

Figure 9. TG analysis on the weight loss of NiO modified STO (a) and LST44 (b) when reduced in 5% H_2 to 900 °C. Infiltrated powder sample was heated in air at 700 °C for 3 h to form NiO phase before TG test.

To compare the interaction between Ni and different substrates, TG analysis was employed to study the reducibility of NiO on LST44 surface compared with STO. In both LST44 and STO substrate, NiO was easier to be reduced when calcined at lower temperature. This may result from particle size of produced NiO. As we mentioned in Figure 6, high annealing temperature in air results in larger NiO particle size, these large particles are more difficult to be reduced than the small ones. The microstructure of Ni modified LST44 powder after TG analysis also suggested the growth of particle size as calcination temperature increase (Figure 10).

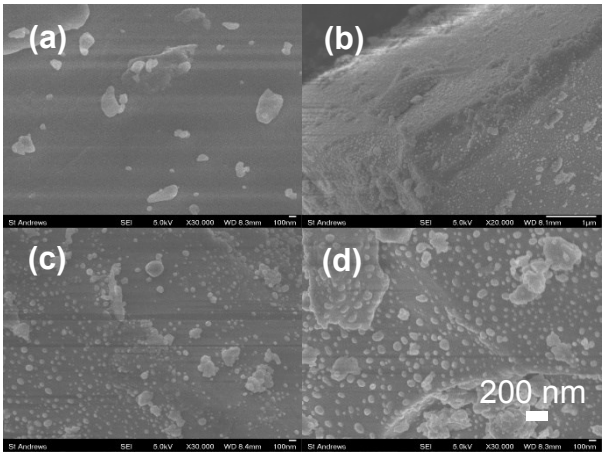

Figure 10. Surface morphology of Ni infiltrated LST44 powder after TG analysis: (a) LST44 without Ni infiltration; (b) LST44 infiltrated NiO at 500 °C; LST44 infiltrated NiO at 700 °C; (d) LST44 infiltrated NiO at 900 °C.

For the STO samples, the last period of mass loss is slower than the beginning, which may indicate some agglomeration of NiO on STO surface. On the contrary, the mass loss of LST44 samples are much more rapid. This could because the NiO on LST44 surface has better distribution and uniform particle size. Moreover, the mass loss, which comes from the loss of oxygen in NiO, changes when heated in different temperature. On STO surface, three samples show almost same oxygen loss, which means the reduced NiO amounts are same. While, on the LST44 surface, heat treatment at higher temperature in air decreased the mass loss a bit. Since the Ni loading amounts of these three samples were controlled to be same in advance, the expected weight loss in three samples should be same, as shown in the STO case. Therefore, one explanation for the lower mass loss is some Ni diffuses into the perovskite lattice because of the existence of A-site deficiency. These de-solved Ni cations can introduce in-lattice bonded oxygen anions, which are much more difficult to be reduced than those in rock salt structure [14]. Our recently study on exsolution materials suggested that B site cation in perovskite structure can transport via A-site vacancy when reducing at high temperature. Although there is no direct evidence for Ni diffusion during infiltration, we believe that A-site deficiency can promote interaction between transition metal and perovskite oxide.

4. Conclusions

In this study, A-site deficient perovskite LST44 was used as Ni infiltration substrate and compared with stoichiometric one STO. Based on the crystal structure characterization, we found that A-site deficiency can promote cation diffusion in sintering process. Further study by TG analysis indicates some Ni cation may dissolve in the perovskite lattice because of A-site deficiency. Further confirmation on Ni cation transport during infiltration process is necessary, but we believe that this is a new strategy to obtain strong metal-oxide interface in infiltrated electrode.

Acknowledgements

The authors would like to thank EPSRC Platform (Grant EP/K015540/1) and the Royal Society for Wolfson Merit Award (WRMA 2012/R2) for funding. We also acknowledge support from China Scholarship Council (CSC).

References:

[1] J. T. S. Irvine, D. Neagu, M. C. Verbraeken, C. Chatzichristodoulou, C. Graves and M. B. Mogensen, *Nature Energy,* 2016, **1**, 1-13.

[2] R. J. Gorte, S. Park, J. M. Vohs and C. H. Wang, *Adv. Mater*, 2000, **11**, 1465-1469.

[3] G. Kim, S. Lee, J. Y Shin G. Corre, J. T. S. Irvine, J. M Vohs and R. J. Gorte, *Electrochem. Solid-State Lett*., 2009, **11**, B48-B52.

[4] L. Lu, C. Ni, M. Cassidy and J. T. S. Irvine, *J. Mater. Chem. A,* 2016, **4**, 11708-11718.

[5] G. Kim, G. Corre, J. T. S. Irvine, J. M Vohs and R. J. Gorte, *Electrochem. Solid-State Lett.*, 2008, **11**, B16-B19.

[6] S. P. Jiang, *Materials Science and Engeering A*, 2006, **418**, 199-210.

[7] Y. Okawa, T. Matsumoto, T. Doi and Y. Hirata, *J. Mater. Res.*, 2002, **17**, 2266-2274.

[8] J. H. Kim, D. J. Suh, T. J. Park and K. L. Kim, *Applied Ctalysis A: General,* 2000, **197**, 191-200.

[9] A. Yaqub, C. Savaniu, N. K. Janjua and J. T. S. Irvine, *J. Mater. Chem. A,* 2013, **1**, 14189-14197.

[10] R. Prce, M. Cassidy, J. A. schuler, A. Mai and J. T. S. Irvine, *ECS Transitions*, 2017, **78**, 1385-1395.

[11] D. Neagu, T. S. Oh, D. N. Miller, H. Menard, S. M. Bukhari, S. R. Gamble, R. J. Gorte, J. M. Vohs and J. T. S. Irvine, *Nat. Comm*., 2015, DOI: 10.1038/ncomms9120.

[12] T. S. Oh, E. K. Rahani, D. Neagu, J. T. S. Irvine, V. B. Shenoy, R. J. Gorte and J. M. Vohs, *J. Phys. Chem. Lett*., 2015, **6**, 5106-5110.

[13] C. J. Howard, G. R. Lumpkin, R. I Smith and Z. Zhang, *J Solid-State Chem*., 2004, **177**, 2726-2732.

[14] D. Neagu, G. Tsekouras, D. N. Miller, H. Menard and J. T. S. Irvine, *Nat. Chem.*, 2013, **5**, 916-923.